JOURNAL OF Materials CHEMISTRY

Powder neutron diffraction studies of three low thermal expansion phases in the NZP family: $K_{0.5}Nb_{0.5}Ti_{1.5}(PO_4)_3$, $Ba_{0.5}Ti_2(PO_4)_3$ and $Ca_{0.25}Sr_{0.25}Zr_2(PO_4)_3$

David A. Woodcock,[a] Philip Lightfoot*[a] and Ron I. Smith[b]

[a]*School of Chemistry, University of St. Andrews, Purdie Building, North Haugh, St. Andrews, Fife, UK KY16 9ST. E-mail: pl@st-and.ac.uk*
[b]*The ISIS Facility, CLRC Rutherford Appleton Laboratory, Chilton, Didcot, Oxfordshire, UK OX11 0QX*

Received 4th May 1999, Accepted 28th July 1999

We present the results of variable temperature neutron powder diffraction studies of three low thermal expansion materials belonging to the NZP family; $K_{0.5}Nb_{0.5}Ti_{1.5}(PO_4)_3$, $Ba_{0.5}Ti_2(PO_4)_3$ and $Ca_{0.25}Sr_{0.25}Zr_2(PO_4)_3$. Each of these structures has half occupancy of the crystallographic site for the large cation (MI = K, Ba or Ca/Sr), but differ in that the vacancies on this site are disordered in the former two (space group $R\bar{3}c$) but ordered in the latter (space group $R\bar{3}$). The thermal expansion behaviour is quantified from parameters obtained by Rietveld structure refinement, and is described in terms of rotations and distortions of linked MO_6 (M = Nb, Ti, Zr) and PO_4 polyhedra. The driving force for the anisotropic low thermal expansion behaviour is found to be in the thermal expansivity of the MI–O bonds. This behaviour is intricately linked to the order/disorder behaviour of the MI sites, as shown by a comparison of the three title structures, together with those of $NaTi_2(PO_4)_3$ in which the MI sites are completely filled, and $Sr_{0.5}Ti_2(PO_4)_3$, in which the MI sites are half-occupied in an ordered manner.

Introduction

Phases with the $NaZr_2(PO_4)_3$ (NZP) structure remain the most widely studied of the known low and negative thermal expansion materials.[1] More recent developments in this field have included microporous materials such as the pure silica zeolites ITQ-3,[2] chabazite[3] and faujasite,[4] the aluminophosphates AlPO-5[5] and AlPO-17,[6] ZrW_2O_8[7] and materials with the scandium tungstate structure such as $Sc_2(WO_4)_3$,[8] and $Y_2(WO_4)_3$.[9] However, the NZP structure is chemically the most versatile. From the basic $NaZr_2(PO_4)_3$ unit, substitutions are possible at the Na site (A = Li, K, $Ca_{0.5}$, $La_{0.33}$ *etc.*), at the Zr site (M = Ti, Hf) and at the P site (X = Si, S). Such substitutions allow tailoring of thermal expansion properties.[10] NZP crystallises in the rhombohedral space group $R\bar{3}c$, the structure consisting of vertex linked ZrO_6 octahedra and PO_4 tetrahedra forming chains aligned up the *c* axis. The Na cation occupies trigonal antiprismatic MI sites also aligned up the *c* axis (Fig. 1). The MII sites, which are situated outside the chains, remain empty. Substitution of the monovalent Na cation by a divalent cation such as Ca or Sr creates an ordering of cations and vacancies in the MI sites (labelled MIa and MIb in Fig. 1), lowering the symmetry to $R\bar{3}$.

The thermal expansion in the system is notable for its anisotropy, with, in general, a contraction of the *a* axis and an expansion of *c* within the $R\bar{3}c$ systems and a reversal of this trend in the $R\bar{3}$ systems. The material $Ca_{0.5}Zr_2(PO_4)_3$ (CaZP) is an exception, crystallising in space group $R\bar{3}$ yet exhibiting $R\bar{3}c$ style thermal expansion properties. Limaye *et al.*[11] synthesised the material $Ca_{0.25}Sr_{0.25}Zr_2(PO_4)_3$ (CaSrZP), which combined the behaviour of CaZP with the more conventional $R\bar{3}$ behaviour of SrZP to create an essentially zero expansion material. Other materials, such as $(Sr_{1-x}K_{2x})Zr_4(PO_4)_6$,[12] result by forming solid solutions between end member phases having $R\bar{3}$ and $R\bar{3}c$ space groups.

The mechanism of thermal contraction within these systems is under investigation. Alamo has proposed a model based on coupled rotations of the polyhedral network.[13] The model is based on changing the size of the trigonal antiprism around the Na position, and was originally proposed to explain the variation of lattice parameters between different members of the NZP series. When a substitution of Na by a larger ion is made (*e.g.* K, forming KZP) the unit cell contracts in the *a*-direction and expands in the *c*-direction. Similarly, when the Na–O bond length increases with T, coupled rotations of the TiO_6 and PO_4 polyhedra lead to an expansion in *c* and a contraction in *a*.

Detailed structural investigations have been limited until recently, with only an X-ray powder diffraction study of $NaTi_2(PO_4)_3$ (NaTP) at five temperatures between 25 and

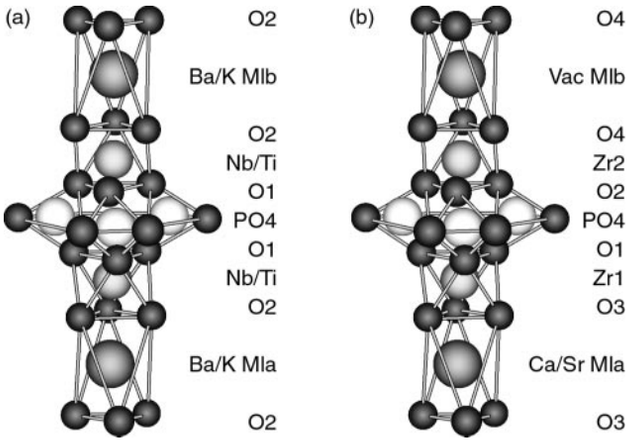

Fig. 1 (a) Portion of the ideal NZP structure showing packing of polyhedral units along the *c*-axis. In both KNTP and BaTP the MIa sites are half occupied. (b) In CaSrZP the MIa site (0,0,0) is fully occupied containing either a Ca or Sr cation, while the MIb site (0,0,1/2) is vacant. The parameter *D* refers to the distance between adjacent O2 planes along the *c*-axis.

800 °C,[14] a neutron powder diffraction study of $Ca_{0.5}Zr_2(PO_4)_3$ (CaZP) at only two temperatures,[15] and a neutron powder diffraction study of $NaSn_2(PO_4)_3$ at four temperatures.[16] Recently, we carried out detailed powder neutron diffraction studies on NaTP, SrTP[17] and LaTP[18] in which we proposed that the differing behaviour of the $R\bar{3}c$ and $R\bar{3}$ systems was due to opposite expansivities of filled and vacant MI sites. It has been suggested by Kutty *et al.*[19] that in materials where a contraction of the *c* axis occurs, this may be due to a disordering of the MI cations, which relocate to MII sites on increasing temperature. However, our previous studies on LaTP showed no such disorder. One question that remained open after our work was whether the *ordering* of filled and vacant MI sites was critical to the anisotropic thermal expansion properties or merely their partial occupancy *per se*. In this work, we aim to investigate the effect of disordering of cations and vacancies in these sites in order to explore this latter question. It has been suggested that $Ba_{0.5}Ti_2(PO_4)_3$ (BaTP) crystallises in the $R\bar{3}$ structure, having half occupied but disordered MI sites.[20] We have also prepared $K_{0.5}Nb_{0.5}Ti_{1.5}(PO_4)_3$ (KNTP) which displays similar behaviour. We present results of powder neutron diffraction studies on both these materials, and compare them to the previously studied SrTP and the 'zero expansion' material CaSrZP, both of which have $R\bar{3}$ structures, with ordered cation vacancies.

Our results are analysed in terms of the Alamo model[13] of polyhedral rotations and distortions, and also in terms of the thermal evolution of the key interpolyhedral Ti–O–P angles. This approach has been used by Evans *et al.*[8] in interpreting the behaviour of $Sc_2(WO_4)_3$.

Experimental

Samples were synthesised using stoichiometric quantities of K_2CO_3 (Aldrich, 99+%), TiO_2 (Aldrich, 99.9+%), Nb_2O_5 (Aldrich, 99.99%), $CaCO_3$ (Aldrich, 99+%), $SrCO_3$ (Aldrich, 98+%), ZrO_2 (Aldrich, 99%), $BaCO_3$ (Aldrich, 99+%) and $(NH_4)_2HPO_4$ (Aldrich, 99%). Starting materials were dried and ground under acetone before being heated to 200 °C for 18 h, 600 °C for 6 h and 900 °C for 12 h. They were then fired for their own individual heat treatment with intermediate regrinding. For $K_{0.5}Nb_{0.5}Ti_{1.5}(PO_4)_3$, (KNTP) this consisted of 24 h at 1000 °C followed by 72 h at 1100 °C, 24 h at 1200 °C and 2 h at 1300 °C; for $Ba_{0.5}Ti_2(PO_4)_3$ (BaTP) 24 h at 1000 °C, 72 h at 1100 °C and 48 h at 1200 °C; and for $Ca_{0.25}Sr_{0.25}Zr_2(PO_4)_3$ (CaSrZP) 48 h at 1200 °C followed by 16 h at 1340 °C. Sample purity was checked on a Stoe Stadi-P powder diffractometer operating in transmission mode using Cu-Kα_1 radiation.

Time-of-flight powder neutron diffraction data were collected from BaTP and KNTP on the Polaris diffractometer[21] while CaSrZP was run on the HRPD diffractometer, both at the ISIS facility, CLRC Rutherford Appleton Laboratory. For each material *ca.* 5 g of sample were loaded into a thin walled vanadium sample can and diffraction patterns collected at room temperature and from 200 to 800 °C in 100 °C steps. Diffraction patterns typically consisted of 4400 data points, 38 variables and 4457 reflections over a *d*-spacing range of 0.5–3.5 Å for both samples run on Polaris and 6267 data points, 63 variables and 1004 reflections over a *d*-spacing range of 0.8–2.5 Å for CaSrZP on HRPD.

Structure refinement was carried out by the Rietveld method using the GSAS program,[22] with the experimentally observed peak shapes modelled by a convolution of pseudo-Voigt and exponential functions. Anisotropic temperature factors were applied for all atoms. A typical profile fit after Rietveld refinement is shown in Fig. 2.

Results and discussion

(i) Coefficients of thermal expansion

The unit cell parameters and atomic coordinates at the highest and lowest temperatures are shown in Tables 1–3. Plots of the behaviour of unit cell parameters and volume are shown in Fig. 3–5. As can be seen the behaviour of all parameters is non-linear. Polynomial coefficients of thermal expansion were therefore calculated using eqns. (1) and (2).

$$p = p_2T^2 + p_1T + p_0 \quad (1)$$

$$\alpha = (p_1 + 2p_2T)/p \quad (2)$$

The term p represents the parameters a, b, c or V, α is the coefficient of thermal expansion and p_2, p_1 and p_0 are polynomial parameters used to fit the data. The resulting values for each material are tabulated in Table 4.

BaTP was the first material chosen to investigate the effect of order of cations and vacancies on the thermal expansivity. It shows an expansion of the *c* axis, contrary to that seen in SrTP, suggesting that the ordering of MI cations and vacancies, onto MIa and MIb sites respectively in SrTP is influential in allowing any behaviour other than expansion along the *c* axis, rather than the half-occupied MI sites found in BaTP. This can

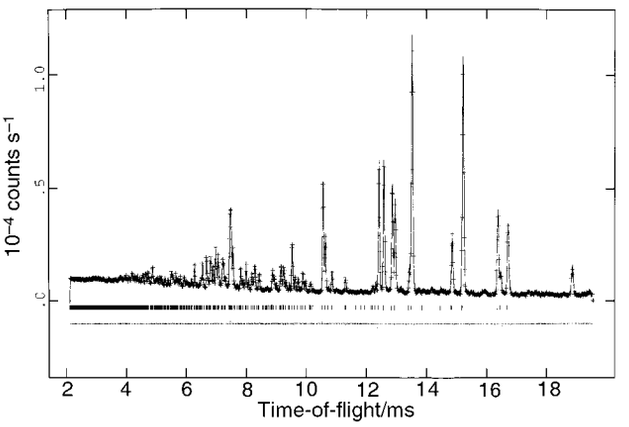

Fig. 2 A typical Rietveld plot for $Ba_{0.5}Ti_2(PO_4)_3$ at 20 °C. Observed (+), calculated (−) profile. Tic marks beneath the diffractogram represent the allowed Bragg reflections. The difference spectrum is located at the bottom of the figure.

Table 1 Experimentally determined atomic coordinates for $K_{0.5}Nb_{0.5}Ti_{1.5}(PO_4)_3$ at 20/700 °C[a]

Atom	Site	*x*	*y*	*z*	*U*(equiv.)/Å^2	Occupancy
K	6b	0	0	0	2.46(9)/7.88(9)	0.5
Nb	12c	0	0	0.1539(1)/0.1535(1)	0.57(9)/2.57(9)	0.25
Ti	12c	0	0	0.1539(1)/0.1535(1)	0.57(7)/2.57(9)	0.75
P	18e	0.2823(2)/0.2828(2)	0	0.25	0.39(6)/1.00(9)	1.00
O(1)	36f	0.1580(2)/0.1581(2)	0.9528(2)/0.9524(2)	0.19671(5)/0.19715(7)	1.35(6)/3.24(9)	1.00
O(2)	36f	0.1983(2)/0.1982(2)	0.1679(2)/0.1688(2)	0.09732(5)/0.09755(8)	1.28(6)/3.03(9)	1.00

[a]Space group $R\bar{3}c$, $a = 8.4330(2)/8.4282(2)$ Å, $c = 22.7344(5)/22.7626(7)$ Å. $R_{wp} = 0.0301/0.0233$, $R_p = 0.0687/0.0448$, $\chi^2 = 5.473/2.740$. Full listings of anisotropic thermal parameters and bond distances and angles for all three structures are available from the authors.

Table 2 Experimentally determined atomic coordinates for $Ba_{0.5}Ti_2(PO_4)_3$ at 20/800 °C[a]

Atom	Site	*x*	*y*	*z*	*U*(equiv.)/Å^2	Occupancy
Ba	6b	0	0	0	2.78(8)/6.93(9)	0.50
Ti	12c	0	0	0.1491(2)/0.1478(3)	0.67(8)/1.24(9)	1.00
P	18e	0.2828/0.2828(3)	0	0.25	0.39(6)/1.03(9)	1.00
O(1)	36f	0.1551(2)/0.1572(4)	−0.0541(2)/−0.0525(3)	0.19734(4)/0.1976(1)	1.71(5)/3.46(9)	1.00
O(2)	36f	0.1969(2)/0.1968(3)	0.1674(2)/0.1676(3)	0.09845(4)/0.0987(1)	1.68(5)/3.47(9)	1.00

[a]Space group $R\bar{3}c$, a = 8.3418(1)/8.3667(3) Å, c = 23.0101(4)/23.0635(8) Å. R_{wp} = 0.0244/0.0290, R_p = 0.0598/0.0645, χ^2 = 4.107/4.579.

Table 3 Experimentally determined atomic coordinates for $Ca_{0.25}Sr_{0.25}Zr_2(PO_4)_3$ at 16/800 °C[a]

Atom	Site	*x*	*y*	*z*	*U*(equiv.)/Å^2	Occupancy
Ca	3a	0	0	0	3.01(2)/9.65(3)	0.50
Sr	3a	0	0	0	3.01(2)/9.65(3)	0.50
Zr(1)	6c	0	0	0.1490(2)/0.1496(2)	1.39(2)/3.14(3)	1.00
Zr(2)	6c	0	0	0.6433(2)/0.6440(2)	1.57(2)/3.13(3)	1.00
P	18f	0.2922(4)/0.2903(4)	0.0086(5)/0.0045(6)	0.2524(2)/0.2520(2)	1.75(2)/3.32(3)	1.00
O(1)	18f	0.1942(4)/0.1902(5)	0.0019(4)/−0.0075(6)	0.1975(2)/0.1987(2)	2.39(3)/5.58(4)	1.00
O(2)	18f	0.0584(4)/0.0532(6)	−0.1581(4)/−0.1638(5)	0.6964(2)/0.6962(2)	2.69(3)/6.06(4)	1.00
O(3)	18f	0.1794(4)/0.1831(5)	0.1788(4)/0.1755(4)	0.0866(2)/0.0880(2)	2.08(3)/4.72(4)	1.00
O(4)	18f	−0.1653(4)/−0.1688(5)	−0.2187(4)/−0.2145(5)	0.5951(2)/0.5952(2)	2.47(3)/5.48(4)	1.00

[a]Space group $R\bar{3}$, a = 8.72452(3)/8.7279(1) Å, c = 22.3573(4)/23.164(1) Å. R_{wp} = 0.0771/0.0524, R_p = 0.072/0.0504, χ^2 = 1.923/1.396.

be seen by comparing values for the parameter *D*, the 'size' of the MI site in BaTP (*i.e.* between adjacent O2 planes along the *c* axis) *vs.* SrTP. Within BaTP *D* increases from 4.53 to 4.55 Å for each MI site over the temperature range room temperature to 800 °C. This represents a very small expansion compared to the behaviour of the occupied site in SrTP which increases from *ca.* 4.14 to 4.35 Å and the vacancy which contracts from 4.48 to 4.31 Å. In other words, the partial occupancy of the MI sites in BaTP ($R\bar{3}c$) restricts the compression of the vacant sites. In both BaTP and KNTP there was no evidence for less than 50% occupancy of the MI sites, nor location of extraframework cations at any other site, at any temperature studied.

KNTP exhibits unusual behaviour, its volume coefficient of thermal expansion of -5.0×10^{-6} at 20 °C being quite strong before zero contraction at 300 °C, returning to a strong expansion of 5.3×10^{-6} at 700 °C. KNTP also shows a *c* axis expansion, increasing from 22.734 to 22.763 Å, with *D* increasing from 4.425 to 4.441 Å. This, like the behaviour of BaTP shows a very small change compared to that of the fully occupied MI sites in NaTP ($R\bar{3}c$) which expand from 3.90 to 4.08 Å. Finally our investigation of CaSrZP, supposedly a zero expansion material, shows a small but significant volume expansion. This is perhaps due to the differing methods of synthesis: the original method used was a sol–gel preparation,[11] in contrast to our solid state reaction. *D* for the occupied sites increases from 4.00 to 4.08 Å, compared to 4.14 to 4.35 Å for SrTP and for the vacant sites it increases more weakly from 4.39 to 4.41 Å compared to the contraction in SrTP from 4.48 to 4.31 Å. This particular material was originally devised to combine the opposite behaviour of CaZP ($-\alpha_a$, $+\alpha_c$) and SrZP ($+\alpha_a$, $-\alpha_c$). Each occupied MI site either contains one Sr or one Ca ion, so the site behaviour represents an average of the influence of each.

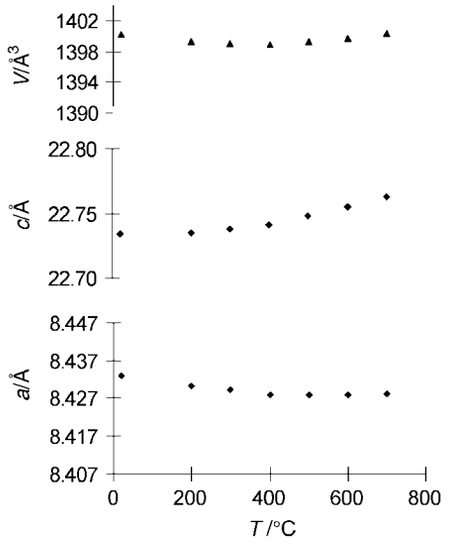

Fig. 3 Thermal evolution of lattice parameters for KNTP. Note that for Figs. 3–5 the scales have been chosen to reflect a similar percentage change.

(ii) The Alamo model

As mentioned earlier, it is the expansion and contraction of the occupied and vacant MI sites which drives the co-operative rotations of linked tetrahedra and octahedra. The Alamo model breaks down the overall expansivity along both the *c* and the *a* axes into individual contributions from the TiO_6 and PO_4 polyhedra. Very little change in the bond lengths within these polyhedra is observed with temperature, and the expansivity is therefore described in terms of rotations and

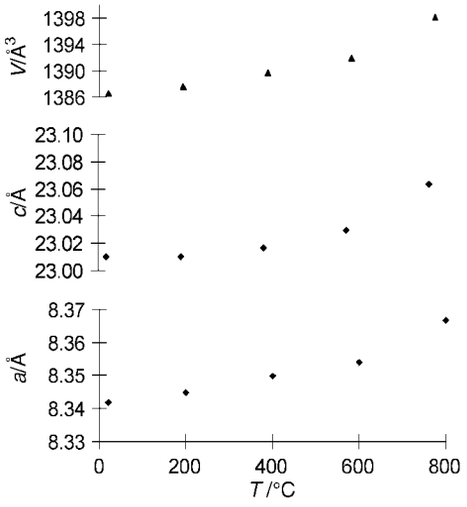

Fig. 4 Thermal evolution of lattice parameters for BaTP.

Table 4 Experimentally determined polynomial parameters

	p_2	p_1	p_0
a_{BaTP}	3.35×10^{-8}	2.81×10^{-6}	8.3423
c_{BaTP}	1.37×10^{-7}	-4.74×10^{-5}	23.012
V_{BaTP}	1.94×10^{-5}	-1.93×10^{-3}	1386.9
a_{KNTP}	-1.735×10^{-8}	-1.977×10^{-5}	8.4344
c_{KNTP}	7.798×10^{-8}	-1.336×10^{-5}	22.734
V_{KNTP}	1.0551×10^{-5}	-7.376×10^{-3}	1400.3
a_{CaSrZP}	4.31×10^{-9}	1.15×10^{-6}	8.7243
c_{CaSrZP}	4.51×10^{-8}	7.01×10^{-5}	23.08
V_{CaSrZP}	4.48×10^{-6}	5.03×10^{-3}	1521.3

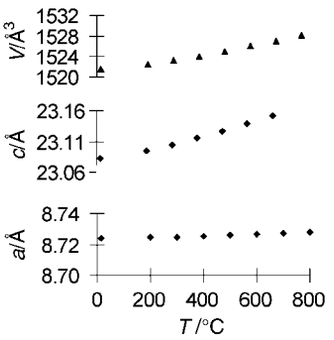

Fig. 5 Thermal evolution of lattice parameters for CaSrZP.

distortions of the polyhedra. The TiO_6 octahedron lies on a three-fold axis along c, and its projection is shown in Fig. 6. $\phi 1$ and $\phi 2$ define rotations of the 'upper' and 'lower' O_3 planes around the c-axis. The PO_4 tetrahedron lies on a two-fold axis in space group $R\bar{3}c$, but this symmetry is lost on reducing to $R\bar{3}$. Corresponding rotation angles in this polyhedron are shown in Fig. 7: $\theta 1$ and $\theta 2$. The angles Ω and Δ are a measure of the distortion of the octahedra and tetrahedra, eqns. (3) and (4).

$$\Omega = \phi 1 - \phi 2 + 60^\circ \quad (3)$$

$$\Delta = \theta 2 - \theta 1 + 90^\circ \quad (4)$$

The expansivities of the TiO_6 and PO_4 polyhedra are insignificant over the temperature range studied. Values of the parameters $\phi 1$, $\phi 2$, $\theta 1$, $\theta 2$, Δ, $\Omega 1$ and $\Omega 2$ for BaTP and KNTP are presented in Fig. 8. The key trends are: for KNTP; $\phi 1$ shows a very slight decrease over the whole range, $\phi 2$ remains constant, leading to an increasing Ω, the octahedron becoming less regular; $\theta 1$ and $\theta 2$ both increasing, leading to a constant Δ, the tetrahedron remaining rigid.

This behaviour shows some parallels to the previously studied NaTP and NbTP systems. $\theta 1$ and $\theta 2$ all increase leading

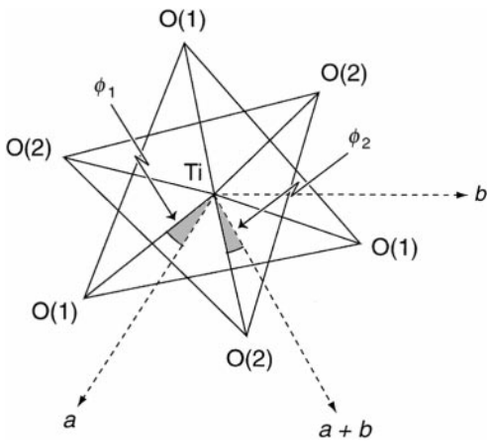

Fig. 6 Projection of a TiO_6 octahedron along the threefold axis (c-axis).

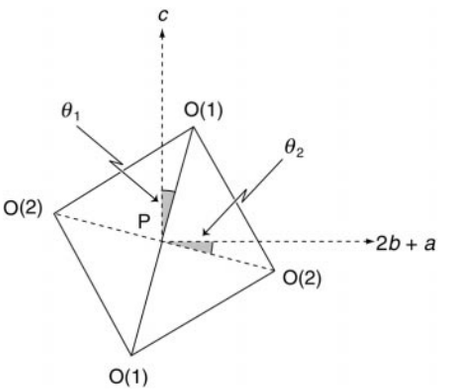

Fig. 7 Projection of a PO_4 tetrahedron along the twofold axis (a-axis).

to a constant Δ, and rigid tetrahedra. Ω increases in all three systems, with increases in $\phi 1$ in both NaTP and NbTP being greater than in KNTP. The increase in NbTP is only marginally greater, but that of NaTP is significantly so, suggesting a correlation between the occupancy of the sites and the strength of rotation.

For BaTP $\phi 1$ decreases and $\phi 2$ remains constant causing Ω to decrease slightly, the octahedron becoming more regular; $\theta 1$ decreases slightly while $\theta 2$ remains constant, leading to an increasing Δ; the tetrahedron becoming more regular. This behaviour is closer to that of SrTP which also shows decreasing Ω and increasing Δ. It must be stressed, however, that in all the cases of BaTP, KNTP and NbTP where there is disordering of the MI vacancies, or completely vacant sites, the magnitudes of *all* the angular changes in the Alamo model are *much* smaller than those in NaTP or SrTP which have completely filled MI or MIa sites. This re-emphasises the fundamental mechanism of the polyhedral rotations being driven by expansion of the MI sites. It is interesting, however that the most significant ϕ rotations occur for $\phi 1$, *i.e.* the O1 face of the TiO_6 octahedron, which is *not* bonded to the MI site.

(iii) Consideration of Ti–O–P angles

The thermal evolution of the Sc–O–W angles has been suggested to be important by Evans *et al.* in $Sc_2(WO_4)_3$ and the corresponding Ti–O–P angles have been considered by us in studies of NaTP and SrTP.[18] NaTP had a negative α_a with the Ti–O1–P angle contracting and SrTP had a positive α_a with the Ti–O1–P angle expanding. The behaviour of the angles in KNTP, CaSrZP and BaTP correlate well with the thermal expansivity. In this study we have considered all of the Ti–O–P angles: in the $R\bar{3}c$ cases there are two; Ti–O1–P and Ti–O2–P which are plotted in Fig. 9. An opening of both of these angles would reflect an expansion of the a axis. Within KNTP, neither Ti–O1–P or Ti–O2–P change significantly, correlating with the minimal expansion of the a axis. Within BaTP, both Ti–O1–P and Ti–O2–P increase slightly. Within the $R\bar{3}$ systems there are four angles. It is the angles associated with the MI sites (Zr–O3–P and Zr–O4–P, Fig. 10) which vary most strongly in

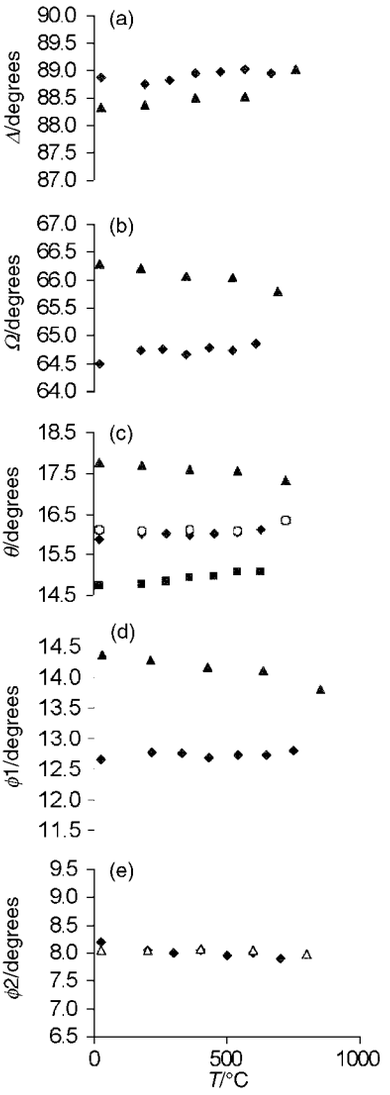

Fig. 8 Variation of the parameters from the Alamo model: (a) Δ_{KNTP} (◆), Δ_{BaTP} (▲); (b) Ω_{KNTP} (◆), Ω_{BaTP} (▲); (c) $\theta1_{KNTP}$ (◆), $\theta2_{KNTP}$ (■), $\theta1_{BaTP}$ (▲), $\theta2_{BaTP}$ (○); (d) $\phi1_{KNTP}$ (◆), $\phi1_{BaTP}$ (▲); (e) $\phi2_{KNTP}$ (◆), $\phi2_{BaTP}$ (△).

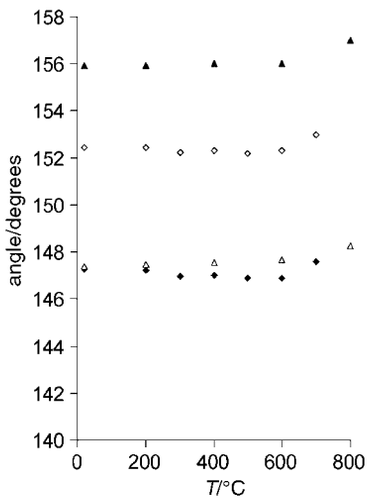

Fig. 9 Thermal evolution of the interpolyhedral Ti–O1–P and Ti–O2–P angles for KNTP (◆, ◇) and BaTP (△, ▲).

CaSrZP, both of which undergo a 2° expansion over the range 20–800 °C. In SrTP the strongest change was in the angles around the Ti(1) site (*i.e.* associated with only the occupied MI site. Ti–O1–P varies from 152.7 to 162° and Ti–O3–P from 143.4 to 155.3°. This differing, and much more pronounced effect is due to either the mixed occupancy of Ca and Sr on the MI sites or substitution of Zr for Ti [we note that in the series $A_{0.5}M_2(PO_4)_3$ (A = Ca, Sr; M = Ti, Zr, Hf, Sn)] the thermal expansion coefficients are strongly influenced by the nature of M.[19]

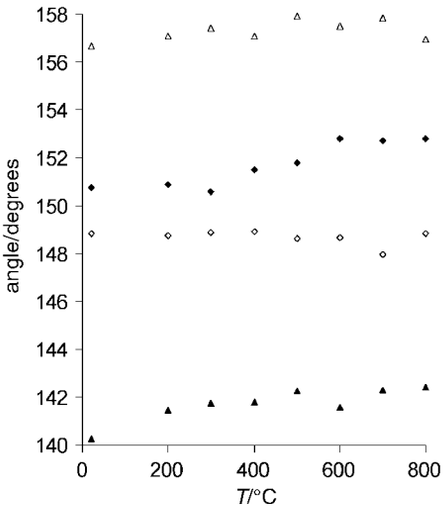

Fig. 10 Thermal evolution of the interpolyhedral Zr–O1–P (△), Zr–O4–P (◆), Zr–O2–P (◇) and Zr–O3–P (▲) angles for CaSrZP.

In NaTP we noted that the negative α_a appears to correlate with the contraction of the Ti–O1–P angle. However, in that case, the Ti–O2–P angle expands by a similar amount. Hence, whether these interpolyhedral angles can be considered as a useful parameter in describing the thermal expansion behaviour of the NZP family is still an open question. A future paper will explore this question in the series $MTi_2(PO_4)_3$ (M = Li, Na, K).

Conclusions

Preparation and study of the samples KNTP and BaTP with disordering on the MI sites has revealed that both materials, although low expansion, do exhibit a significant *c* axis expansion on heating. Ordering of cations and vacancies, as occurs in the $R\bar{3}$ phase SrTP which exhibits zero *c*-axis expansivity, appears to be influential in understanding the opposite anisotropy of $R\bar{3}$ and $R\bar{3}c$ structured samples.

It appears that the method of preparation of CaSrZP may affect its properties. Previous studies had revealed this material to be essentially zero expansion when prepared by a sol–gel method. However, our sample, prepared by a solid state method, was found to expand weakly.

Acknowledgements

We would like to acknowledge the EPSRC for provision of a studentship to D.A.W. and funding of neutron beamtime, and Dr Richard Ibberson and Miss Zoe Lethbridge for assistance in collection of neutron diffraction data.

References

1 J. P. Boilot, J. P. Salanie, G. Desplanches and D. Le Potier, *Mater. Res. Bull.*, 1979, **14**, 1469.
2 D. A. Woodcock, P. Lightfoot, P. A. Wright, L. A. Villaescusa, M.-J. Díaz-Cabañas and M. A. Camblor, *J. Mater. Chem.*, 1999, **9**, 349.
3 D. A. Woodcock, P. Lightfoot, L. A. Villaescusa, M.-J. Díaz-Cabañas, M. A. Camblor and D. Engberg, *Chem. Mater.*, in press.
4 M. P. Attfield and A. W. Sleight, *Chem. Commun.*, 1998, 601.

5 S. H. Park, R. W. Große Kunstleve, H. Graetsch and H. Gies, *Stud. Surf. Sci. Catal.*, 1997, **105**, 1989.
6 M. P. Attfield and A. W. Sleight, *Chem. Mater.*, 1998, **10**, 2013.
7 J. S. O. Evans, T. A. Mary, T. Vogt, M. A. Subramanian and A. W. Sleight, *Chem. Mater.*, 1996, **8**, 2809.
8 J. S. O. Evans, T. A. Mary and A. W. Sleight, *J. Solid State Chem.*, 1998, **137**, 148.
9 D. Woodcock, P. Lightfoot and C. Ritter, *J. Solid State Chem.*, in press.
10 R. Roy, D. K. Agrawal and H. A. McKinstry, *Annu. Rev. Mater. Sci.*, 1989, **19**, 59.
11 S. Y. Limaye, D. K. Agrawal and H. A. McKinstry, *J. Am. Ceram. Soc.*, 1987, **70**, C232.
12 D. K. Liu, L.-J. Lin and C.-J. Chen, *J. Appl. Crystallogr.*, 1995, **28**, 508.
13 J. Alamo, *Solid State Ionics*, 1993, **63–65**, 547.
14 J. L. Rodrigo, P. Carrasco and J. Alamo, *Mater. Res. Bull.*, 1989, **24**, 611.
15 J. Alamo and J. L. Rodrigo, *Solid State Ionics*, 1993, **63–65**, 678.
16 J. Alamo and J. L. Rodrigo, *Mater. Res. Bull.*, 1992, **27**, 1091.
17 D. A. Woodcock, P. Lightfoot and C. Ritter, *Chem. Commun.*, 1998, 107.
18 P. Lightfoot, D. A. Woodcock, J. D. Jorgensen and S. Short, *J. Inorg. Mater.*, 1999, **1**, 53.
19 K. V. G. Kutty, R. Asuvathraman and R. Sridharan, *J. Mater. Sci.*, 1998, **33**, 4007.
20 C. Y. Huang, D. K. Agrawal and H. A. McKinstry, *J. Mater. Sci.*, 1995, **30**, 3509.
21 R. I. Smith and S. Hull, User Guide for the Polaris Powder Diffractometer at ISIS, Report RAL-TR-97-038, Rutherford Appleton Laboratory, 1997.
22 A. C. Larson and R. B. Von Dreele, Los Alamos National Laboratory Report No. LA-UR-86-748, 1987.

Paper 9/03489G